Roles of resonances and recollisions in strong-field atomic phenomena: Above-threshold ionization

Joseph Wassaf, Valérie Véniard, Richard Taïeb, and Alfred Maquet
Laboratoire de Chimie Physique-Matière et Rayonnement, Université Pierre et Marie Curie, 11, Rue Pierre et Marie Curie, 75231 Paris Cedex 05, France

(Received 24 February 2003; published 28 May 2003)

We present the results of a set of quantal and classical calculations designed for simulating the photoelectron spectra observed when atoms are submitted to an intense laser field. We have concentrated the discussion on the range of parameters where conspicuous enhancements are observed in the high-energy part of the above-threshold ionization (ATI) spectra. Our results confirm that these enhancements result from a resonant transfer of population into the Rydberg states. Subsequent multiple returns, with elastic or inelastic recollisions of the electrons with the nucleus, when they are released in the continuum, also play an essential part. Our analysis highlights also the similarities as well as the differences observed in simulations, depending on the choice of the model potential, i.e., if it is either long range (Coulomb-like) or short range (with an exponentially decreasing tail).

DOI: 10.1103/PhysRevA.67.053405 PACS number(s): 32.80.Rm

I. INTRODUCTION

When atoms are submitted to intense infrared laser pulses with peak intensities around $I \approx 10^{14}$ W cm^{-2}, the energy distributions of the fast photoelectrons can exhibit strong variations, up to one- (or even two-) order(s) of magnitude, when the peak intensity changes by only a few percents [1–3]. A simulation of this behavior is shown below in Fig. 1. These changes are observed in the high-energy part of the above-threshold ionization (ATI) spectra, comprised between $2U_p$ and $10U_p$ [4]. Recent experiments have also evidenced strong variations in the contrast of the ATI peaks in the same energy range [5]. It is now understood that these fast electrons have experienced at least one rescattering event from the ionic core, while they are driven by the oscillating field [6]. The physical basis of this interpretation is that the electrons released directly in the continuum, via tunnel ionization, cannot acquire more than $2U_p$ in kinetic energy. It is only in the course of a rescattering process that they can gain more energy (up to $10U_p$), in the presence of the laser field. In the context of this well-established semiclassical interpretation, the existence of the above-mentioned variations of magnitudes of a subset of ATI peaks could not be interpreted. The main objective of the present study was to investigate the physical processes responsible for the occurrence of these features.

Soon, it was realized that these effects could be related to the structure of the atomic system considered. This was clearly evidenced in a series of papers devoted to the interpretation of experiments conducted on Ar atoms submitted to Ti:sapphire laser pulses ($\omega = 0.0577$ a.u. ≈ 1.57 eV and time durations $\tau \approx 120$ fs) [7]. Indeed, by solving the time-dependent Schrödinger equation (TDSE) for a model argon atom, it has been possible to reproduce the high-energy structures in the photoelectron spectra with remarkable agreement. The calculations were performed, within the framework of a single active electron approach, with the help of a fit of an Hartree-Fock potential which could reproduce the energy spectrum of the dominant excited states with good precision. The physical interpretation deduced from these simulations was that the photoelectrons pertaining to the peaks considered had experienced a resonant transition involving Rydberg states [8,9]. The highly nonlinear dependence of the magnitude of the structures in terms of the laser intensity, was interpreted as resulting from the fact that population transfers from the ground state to the Rydberg states—through multiphoton resonant transitions—could take place only in narrow intensity windows.

However, several objections have been raised against this interpretation. One is that the resonant Rydberg states have energies located well above the effective barrier resulting from the combination of the atomic potential and of the laser field. The lifetimes of these states were expected to be extremely short, as they could be ionized within a fraction of a laser cycle. It is then difficult to explain how such short-lived states could play a determining role in the ionization dynamics and how they could induce a resonantlike behavior observable only in the high-energy tail of the ATI spectra. Another question was to reconcile this interpretation with the recollision mechanism, which is known to account for this part of the spectra.

In the meantime, another set of simulations have led to a different interpretation, based on the occurrence of a ''channel-closing'' mechanism. Indeed, very similar enhancements are found also, with simplified models using a zero-range (delta-function) potential that supports only one bound state [10–12]. These observations are based on approaches derived from the *S*-matrix formalism, including only bound-free transitions, i.e., with no reference at all to any resonant effect involving excited states. Also, a fully nonperturbative approach, based on the analytical determination of the Floquet quasienergies for the same type of potential, confirms these findings [13]. And, very recently, the resonant behavior of the ionization threshold has been ascribed to the occurrence of interfering quantum orbits associated with zero-energy states [14]. All these simulations point to a channel-closing effect, related to the increase in the integer number of photons required to ionize the atom when the field strength is growing. This is a direct consequence of the fact that, within the field, the ionization energy

grows almost proportionally to U_p. In the absence of excited states, the zero-energy limit of the continuous spectrum, with its associated discontinuity in the density of states, is the only feature that can be responsible for a pseudoresonance with the ground state. This entails that the ionization rates do exhibit abrupt changes at each threshold, a behavior which could account for the observed spectra. It should be noted that similar enhancements have been found also when simulating, with the help of the same kind of approach, high harmonic generation spectra, Ref. [15], see also Ref. [16].

One limitation of this class of calculations, based on zero-range potentials with no excited states, is that they are better suited to model the response of negative ions, instead of atoms. In the latter systems, in which the experimental observations of the effect have been realized, the long-range character of the effective atomic potential favors the possibility of observing resonant processes. It is thus of interest to investigate why two distinct types of models could reproduce the presence of the observed enhancements, in spite of the fact that they are *a priori* very different from each other and that they lead to different interpretations of the physical mechanism at work.

In order to address this puzzling question, we have performed a set of quantal and classical simulations for two classes of one-dimensional model potentials, either long range, with a Coulomb tail, or short range, with an exponential decay [17]. As explained in the following, our results validate the scenario based on a multiphoton resonance on the Rydberg states in atomic systems. Also, they shed light on the reasons why the simulations based on the zero-range model potential can mimic the behavior observed in experiments. Indeed, one also finds marked enhancements at intensities very close to (in fact slightly below) those corresponding to channel closings. But, even more interestingly, our numerical simulations reveal the presence of the so-called laser-induced states (LIS) [18,19]. Our calculations show that they can play a role similar to that played by the Rydberg states in a long-range potential. We believe that, although they do not represent ''the end of the story,'' this set of results bring new informations on the physical mechanisms responsible for this class of phenomena.

The organization of the paper is as follows: In the following section, we shall present a set of simulations performed for investigating the dynamics of ionization in a single-active electron atom system, modeled with the help of a long-range potential. Three subsections are devoted to the presentation of the results of (i) a time-dependent Schrödinger equation (TDSE) treatment, (ii) a Floquet quasienergy treatment, and (iii) classical trajectories simulations. In Sec. III are presented a set of quantal (TDSE and Floquet) simulations, performed for short-range potentials, modeling the dynamics of ionization in negatively charged ions. Section IV is devoted to the discussion of the results we have obtained for the two types of potentials and to a general discussion.

Note that we shall discuss the occurrence of the same class of resonant effects in harmonic generation in a follow up of the present paper [16].

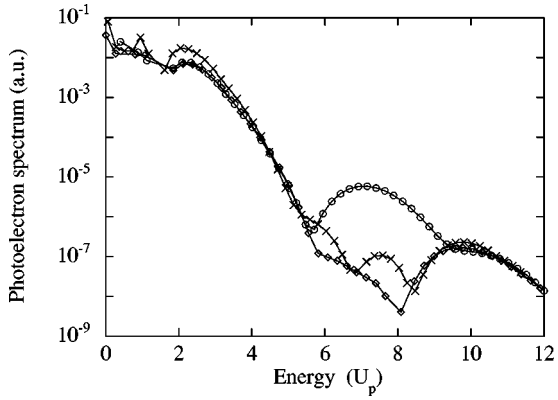

FIG. 1. Photoelectron spectra for the long-range potential Eq. (1) and for $\omega=0.0577$ a.u. Open circles, diamonds, and crosses correspond to intensities of 1.12×10^{14} W cm^{-2}, 1.02×10^{14} W cm^{-2}, and 1.22×10^{14} W cm^{-2}, respectively. The pulse duration is $18T_L$.

II. LONG-RANGE POTENTIAL: PHOTOIONIZATION DYNAMICS IN THE PRESENCE OF RYDBERG STATES

A. Time-dependent Schrödinger equation (TDSE) treatment

In order to model the response of an atomic electron, we have used the so-called ''soft-Coulomb'' potential [20]:

$$V(x)=-\frac{1}{\sqrt{c+x^2}}, \tag{1}$$

which behaves asympotically as a one-dimensional Coulomb potential and supports an infinite number of bound states. With $c=1.41$, the ground-state energy is the same as for Ar atoms: $\epsilon_0=-0.58$ a.u. This class of potentials has been shown to be useful to reproduce the main features of laser-atom interactions in the strong-field regime, for a linearly polarized laser.

Examples of the ATI spectra, simulated when the above system is submitted to a trapezoidal laser pulse with frequency $\omega=0.0577$ a.u.≈1.57 eV, with a total duration of 18 cycles including one-cycle turn-on and turn-off, are shown in Fig. 1. The spectra are deduced from the spectral analysis of the final wave function obtained by solving the TDSE [21]:

$$i\frac{\partial}{\partial t}\Psi(x,t)=\left[H_0+i\frac{A(t)}{c}\frac{\partial}{\partial x}\right]\Psi(x,t), \tag{2}$$

where $A(t)$ is the vector potential of the field and

$$H_0=-\frac{1}{2}\frac{\partial^2}{\partial x^2}+V(x). \tag{3}$$

The numerics relies on a standard Crank-Nicholson scheme for the time propagation and a variable step discretization for the space integration [22,23]. The size of the box is large enough for containing the fast components of the wave function. Typical values for the grid spacing is $\Delta x=0.1$ a.u. and

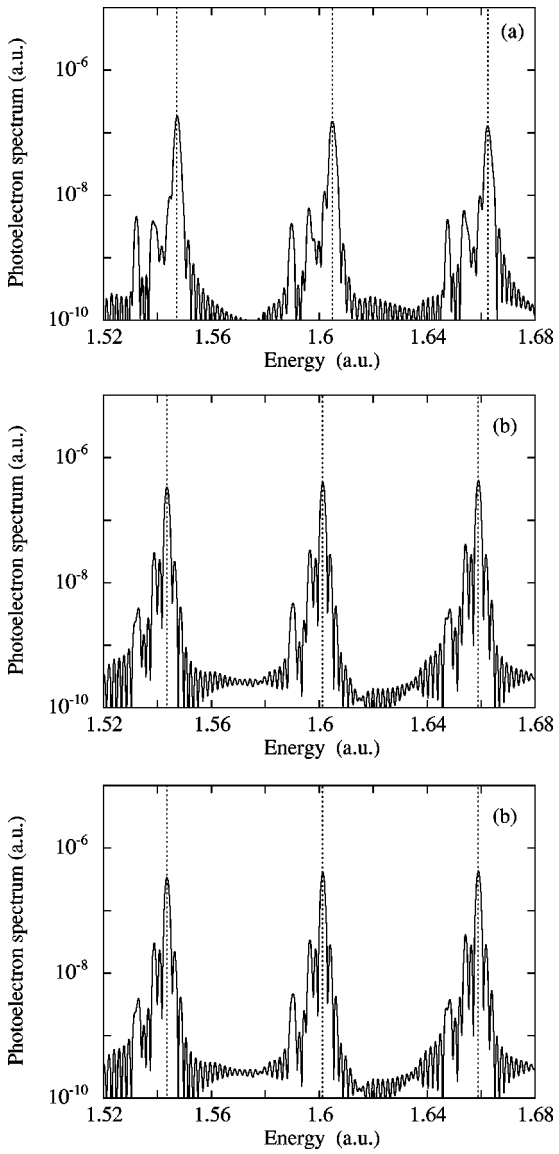

FIG. 2. Enlargement of photoelectron spectra for the long-range potential, Eq. (1), in the same conditions as in Fig. 1. (a) corresponds to an intensity of 1.08×10^{14} W cm^{-2}, (b) to 1.10×10^{14} W cm^{-2}, and (c) to 1.12×10^{14} W cm^{-2}. The enhancement in Fig. 1 is observed at the latter intensity.

we used box size of $\approx$3300 a.u. We have checked that our results are robust while varying these parameters.

In Fig. 1, the ATI spectra for three selected intensities are shown. One can check that, at $I=1.12\times10^{14}$ W cm^{-2}, a conspicuous enhancement shows up in the region comprised between $5.5U_p$ and $9.2U_p$. Conversely, it almost disappears at the neighboring intensities $I=1.02\times10^{14}$ W cm^{-2} and $I=1.22\times10^{14}$ W cm^{-2}.

The structures of three peaks in the central region close to the maximum where the enhancement is observed, are shown in Fig. 2, at intensities close to $I=1.12\times10^{14}$ W cm^{-2}. As observed in the experiments [7], each peak is constituted of several subcomponents. The dominant one corresponds to the energy-conserving multiphoton transition from the ground state. By comparing Figs. 2(a)–2(c), we note that,

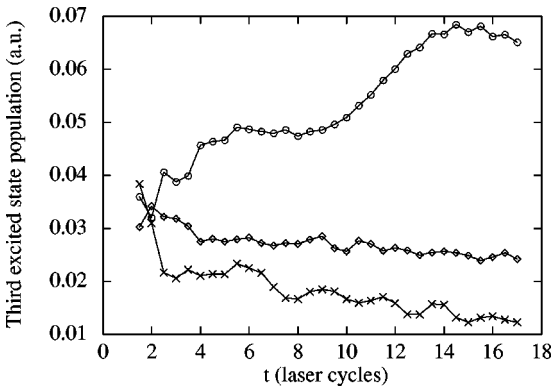

FIG. 3. Projection of the wave function at times odd multiples of $T_L/4$ on the bare state $n=3$ for three different intensities. Diamonds, open circles, and crosses correspond to intensities of 1.02×10^{14} W cm^{-2}, 1.12×10^{14} W cm^{-2} (when the enhancement is observed in Fig. 1), and 1.22×10^{14} W cm^{-2}, respectively.

when the intensity is varied, its position is shifted in proportion. This is because the ionization energy $|\epsilon_0|$ is changing with the field intensity, i.e., with U_p, according to the relation [24]:

$$E_{kin,N}\approx N\omega-|\epsilon_0|-U_p, \tag{4}$$

which represents a good approximation of the kinetic energy of a photoelectron that has absorbed N photons from the ground state. In addition, there are other peaks that do not move appreciably when the intensity is varied. Their presence is a signature of resonant processes involving excited states [7,8], a phenomenon much similar to that observed in the low-energy part of the spectrum, for short laser pulses [25]. One observes that the integrated height of the peak grows considerably at the intensities when the nonresonant subpeak coincides with one of the resonant ones, i.e., when the resonance conditions are met (note the logarithmic scale). This observation accounts for the presence of the enhancement in the ATI spectrum.

In order to assess further the existence of a resonant process, we have monitored the relative population of the third $(n=3)$ excited state, which comes into quasiresonance with the ground state at these intensities (through a 13-photon transition, see below). The resulting variations in time of the projection of the (time-dependent) wave function on the ''bare'' $n=3$ wave function is shown in Fig. 3. One observes a very significant transfer of population developing in time at $I=1.12\times10^{14}$ W cm^{-2}, i.e., when the maximum shows up in Fig. 1 and when the nonresonant peak merges with one of the subpeaks, as verified in Fig. 2.

In spite of the fact that the bare state basis is not really adequate for analyzing the time-dependent wave function of the atom ''dressed'' by the external field (see below), it can provide useful indications on the population dynamics. With this caveat in mind, the results of Fig. 3 confirm the existence of an important transfer of population in the excited state $n=3$ at the intensity when the enhancement is observed. This confirms the hypothesis, presented in Refs. [7–9], of a multiphoton resonance being responsible for the

enhancement. However, it does not explain how it is possible that this resonance with the state $n=3$, with bare energy $\epsilon_3=-0.0888$ a.u., located so high above the ionization barrier in the presence of the field (when $I=1.12\times10^{14}$ W cm^{-2}, the top of the barrier is at $E_{barr}=-0.4659$ a.u.), can lead to so important changes in the spectra. In order to address this question, we have used first a Floquet analysis to determine the shifted energies of the states dressed in the presence of the field and to identify with certainty the resonant states.

B. Floquet quasienergies treatment

The projection of the time-dependent wave function onto those of the atomic stationary states varies constantly in time and there is no completely satisfactory criterion for deciding the significance of the numbers obtained [26]. Another choice, intrinsically more adapted, is to use the basis constituted by the Fourier-Floquet components of the wave function of the system, in the presence of a constant amplitude field [27]. The advantage of the Floquet approach, when combined with the complex rotation of the coordinate, is that it permits to find the complex quasienergies of the system dressed by the field [28,29].

In a constant amplitude, periodic field, with vector potential

$$A(t)=A_0e^{-i\omega t}+\text{c.c.}, \tag{5}$$

the Floquet theorem states that the solutions of the TDSE are of the general form

$$\Psi(x,t)=e^{-i\mathcal{E}t}\sum_{n=-\infty}^{n=+\infty}e^{in\omega t}\phi_n(x). \tag{6}$$

Here, $\mathcal{E}\in\mathbb{C}$ is the so-called ''quasienergy'' and the functions $\phi_n(x)$ are the Fourier-Floquet components of the general solution. The latter are solutions of an infinite system of coupled equations [27]:

$$[H_0+n\omega]\phi_n(x)+i\frac{A_0}{c}\frac{\partial}{\partial x}\phi_{n+1}(x)+i\frac{A_0}{c}\frac{\partial}{\partial x}\phi_{n-1}(x) =\mathcal{E}\phi_n(x). \tag{7}$$

Much in the spirit of the work by Shakeshaft *et al.* [30], to solve this system, we have constructed a basis of Sturmian functions adapted to the soft-Coulomb potential. Starting from the Schrödinger equation for this potential with a given effective charge or, in other words, a coupling constant α:

$$\left(-\frac{1}{2}\frac{\partial^2}{\partial x^2}-\frac{\alpha}{\sqrt{c+x^2}}\right)\psi_n(\alpha,x)=\lambda_n\psi_n(\alpha,x), \tag{8}$$

one defines the associated Sturmian equation

$$\sqrt{c+x^2}\left(\frac{1}{2}\frac{\partial^2}{\partial x^2}+\lambda\right)S_\nu(\lambda,x)=\alpha_\nu S_\nu(\lambda,x), \tag{9}$$

which, for a fixed value of the energylike parameter λ, is an eigenvalue equation for the ''coupling constant'' α [31]. In matrix form, it reads

$$\mathbf{MS}=\alpha\mathbf{S}. \tag{10}$$

For a given λ and with appropriate boundary conditions, the set of Sturmian functions $S_\nu(\lambda,x)$ form a discrete basis. In the case of the Coulomb potential, it has proven itself to be particularly useful in strong-field calculations [30,32,33]. Here, however, for the soft-Coulomb potential, in contrast to the exact Coulomb case, there are no analytical solutions, neither for the Schrödinger equation, nor for the associated Sturmian one (see, however, Ref. [34]), and one has to solve them numerically on a grid. It turns out that the matrix **M** is tridiagonal, with

$$M_{i,i}=\sqrt{c+x_i^2}\left(\frac{1}{\delta x^2}+\lambda\right), \tag{11}$$

$$M_{i,i+1}=-\sqrt{c+x_i^2}\left(\frac{1}{2\,\delta x^2}\right), \tag{12}$$

$$M_{i+1,i}=-\sqrt{c+x_{i+1}^2}\left(\frac{1}{2\,\delta x^2}\right), \tag{13}$$

with $x_{i+1}=x_i+\delta x$. By diagonalizing it, one can obtain the set of eigenvalues α_ν and the corresponding eigenfunctions $S_\nu(x)$. Once the latter are determined, one can diagonalize the Floquet matrix itself, Eq. (7). Before doing so, as a check, we have diagonalized the field-free Hamiltonian H_0 in the Sturmian basis, to derive the energies of the bound states. We note that the number of basis functions required to achieve a given accuracy depends on the choice of the free parameter λ. Typical numbers are that, with 200 basis functions, and $\lambda\in\mathbb{C}$, one easily reproduces the energies of the first 15 states of the soft-Coulomb potential, Eq. (1), with a six-digit accuracy.

As an illustration of the power of the method, we have analyzed in more detail the resonant processes responsible for the enhancement shown in Fig. 1 and for the structures of the ATI peaks shown in Fig. 2. The restriction to a selection of odd-parity excited states of the Floquet spectrum is shown in Fig. 4(a). It permits to evidence clearly the crossing, taking place at $I=1.12\times10^{14}$ W cm^{-2}, between the dressed state evolving from the state $n=3$ with the dressed ground-state energy $\tilde{\epsilon}_0\approx\epsilon_0+13\omega$. In Fig. 4(b), the restriction to the even-parity states of the Floquet spectrum evidences another crossing, taking place exactly at $I=1.145\times10^{14}$ W cm^{-2}, resulting from a 14-photon resonance between the dressed states evolving from the ground $n=0$ and the $n=6$ states. Also at this intensity, a significant enhancement shows up in the ATI spectrum, see Fig. 1 of Ref. [17]. We note that these two resonant enhancements occur without any channel closing in this intensity range.

The presence of these two resonances, taking place at intensities very close to each other, permits to better understand the origin of the subcomponents observed in the ATI

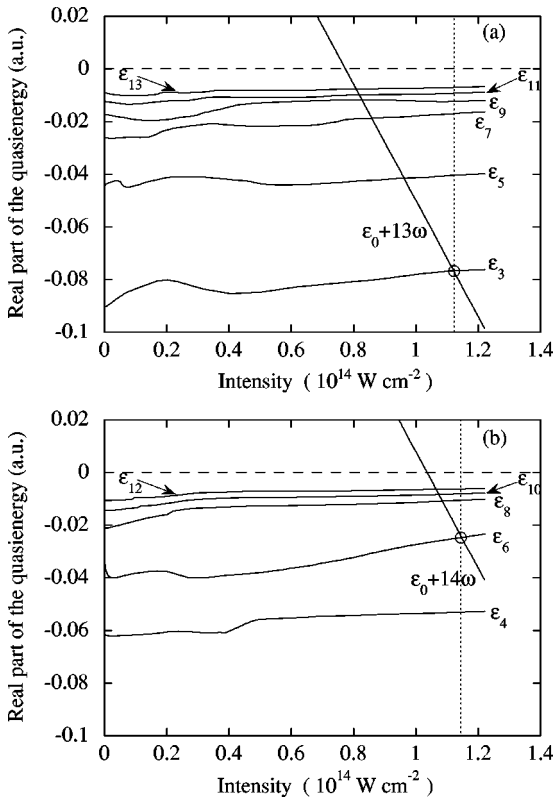

FIG. 4. (a) Odd-parity states quasienergies; (b) even-parity states quasienergies. The crossings between the ground state and the dressed states $n=3$ and $n=6$ occur at intensities 1.12×10^{14} W cm^{-2} and 1.145×10^{14} W cm^{-2}, respectively.

peaks already shown in Fig 2. Enlargements of the structure of one of the peaks are displayed in Fig. 5, where three dominant peaks are identified and their positions at three different intensities are recorded. As explained previously, the one labeled (0), that is moving towards lower energies as the intensity grows, corresponds to the (nonresonant) *N*-photon absorption from the ground state, following Eq. (4). With the help of the Floquet analysis, one can assign the peaks labeled (3) and (6) to a 13-photon resonance with the state $n=3$ and to a 14-photon resonance with the state $n=6$, respectively. One can verify that their positions do not vary significantly in the narrow range of intensity considered here.

To conclude this subsection, the Floquet analysis has permitted to identify, without ambiguity, the excited states participating in the resonant process. They are responsible for the high-energy structures found when simulating the spectra from the TDSE. In that respect, it fully confirms the analysis made by Muller *et al.* [7–9]. We add that we did not find enhancements at intensities located in the vicinity of those associated to channel closings.

C. Classical trajectories simulations

Although the existence of a resonant process leading to the observed structures is confirmed, it remains to explain why they are located at energies centered around $7U_p$ (in the case considered here). The presence of subcomponents in the

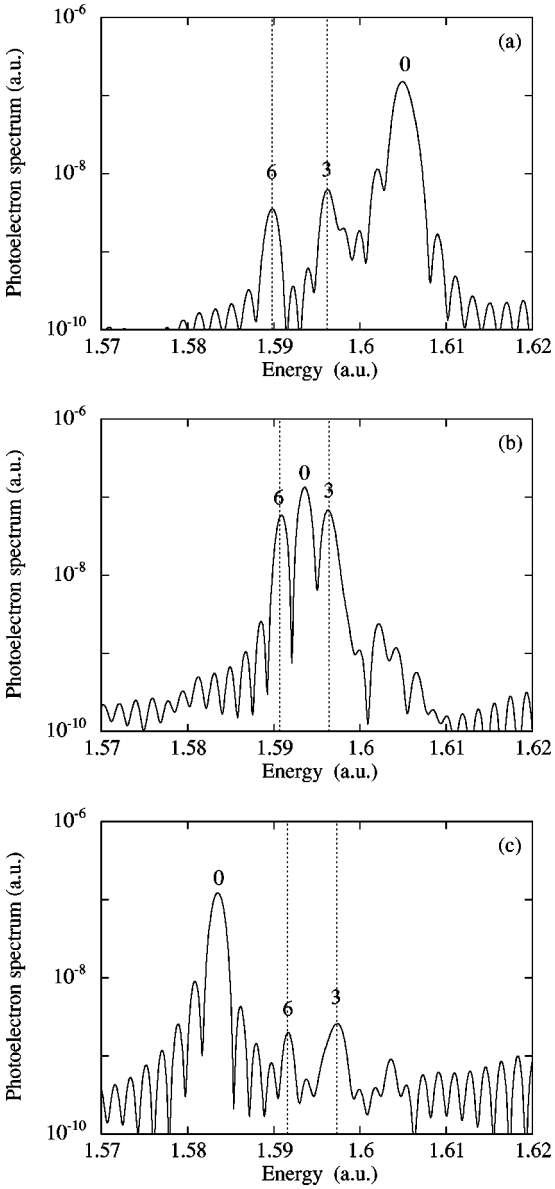

FIG. 5. Details of one photoelectron peak showing subcomponents. (a) corresponds to an intensity of 1.081×10^{14} W cm^{-2}, (b) to 1.135×10^{14} W cm^{-2}, and (c) to 1.180×10^{14} W cm^{-2}. The peak labeled 0 corresponds to the direct ionization process, while the peaks labeled 3 and 6 are associated to Freeman resonances via the dressed states $n=3$ and $n=6$.

ATI peaks is the signature of the occurrence of multiphoton resonances that have been dubbed ''Freeman-resonances'' [25]. They are usually observed in the low-energy part of the spectrum. This indicates that they involve electrons that are ejected directly, without subsequent return to the nucleus. Here, the phenomenon takes place for fast photoelectrons that have experienced at least one recollision with their parent ionic core. The question at hand is to justify the fact that the resonant behavior is not washed out in the subsequent recollision process.

A natural way to investigate this point is to resort to a classical trajectory approach. Indeed, simplified classical trajectory calculations have permitted to explain the dominant

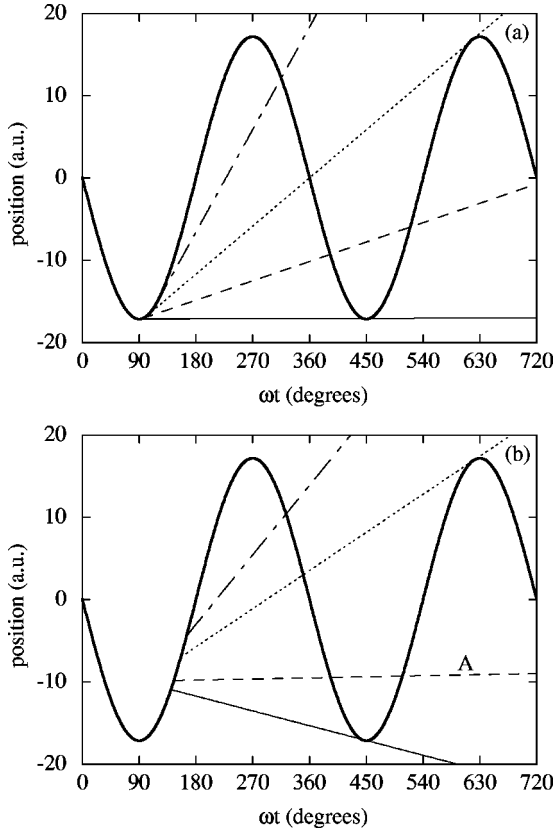

FIG. 6. Graphical determination of return times for different release times at an intensity of 1.145×10^{14} W cm^{-2}. (a) corresponds to the direct tunneling process from the ground state [Eq. (14)], while (b) to the process via the $n=6$ state [Eq. (16)]. The trajectory labeled *A* is almost periodic.

features of the ATI spectra, by computing the energies acquired by the electrons freed into the continuum via tunnel ionization. As already mentioned, one can distinguish two mechanisms leading to two distinct families of photoelectrons. Those detected at energies below $2U_p$ are those which are ejected directly and never come back to the origin. This scheme is by far the most probable, which explains why the dominant ATI contributions to the photocurrent are in the low-energy range. However, a restricted class of trajectories, ejected in a small time window during a laser cycle, can reencounter the origin. Then, depending on the phase of the laser, they can reach energies up to $10U_p$ in the course of the recollision. As already mentioned, they are responsible for the existence of the plateau observed beyond $2U_p$.

This mechanism is graphically illustrated in Fig. 6(a), where a graphical solution for the return times of the electron at the origin is sketched, see Ref. [35]. Since the time dependence of the trajectory is given by

$$x(t)=\frac{F_0}{\omega^2}[\sin(\omega t)-\sin(\omega t_0)]-\frac{F_0}{\omega}(t-t_0)\cos(\omega t_0), \tag{14}$$

where F_0 is the field amplitude, the return times at $x=0$ are given by the intersection of the sinusoid with the straight lines associated to the drift motion of the free electrons. In the case of tunnel ionization, implying a zero initial velocity, the lines are tangent to the sinusoid at the time of ionization. One can check that a fraction of the trajectories can lead to one (several) recollision(s). One also observes that, if the ejection takes place when the field amplitude is the maximum (here it is when the phase of the laser is an odd multiple of $T_L/4$), the electron undergoes an oscillatory motion, coming back each time to the origin with zero velocity.

The situation is much different if the electron is initially in an excited state located above the effective potential barrier. Then, when leaving the atom at t_0, it possesses an initial kinetic energy that can be estimated as the difference between the bound-state energy ϵ_n and the top of the barrier at the time considered:

$$E_{kin}(t_0)=\epsilon_n-E_{barr}(t_0). \tag{15}$$

In this situation, the electrons ejected directly, that never come back to the origin, can acquire energies significantly higher than in the preceding case. For example, if the laser intensity is $I=1.145\times10^{14}$ W cm^{-2}, the electrons with an initial energy $E(t_0)=\epsilon_6\approx-0.0337$ a.u. can reach final energies up to $E_{max}=5.47U_p$. On the other hand, as the electron possesses an initial velocity $v(t_0)=\pm\sqrt{2E_{kin}(t_0)}\neq0$, the trajectories are given by the modified equation:

$$x(t)=\frac{F_0}{\omega^2}[\sin(\omega t)-\sin(\omega t_0)]-\frac{F_0}{\omega}(t-t_0)\cos(\omega t_0)+(t-t_0)v(t_0). \tag{16}$$

The return times can be derived as shown in Fig. 6(b). There is a large class of trajectories that can come back at least one time to the origin. Many of them can experience several recollisions and some can revisit the origin an infinite number of times, with a nonzero kinetic energy. For a recollision occurring at t_1, the instantaneous kinetic energy is given by

$$E_{kin}(t_1)|_{x=0}=\frac{1}{2}\left[\frac{F_0}{\omega}[\cos(\omega t_1)-\cos(\omega t_0)]\pm\sqrt{2E_{kin}(t_0)}\right]^2. \tag{17}$$

Clearly, the electrons following these trajectories have a greater chance to gain further kinetic energy in the course of a recollision. One finds, in particular, that for the same conditions as above, the electrons ejected between $140°<\omega t_0<180°$ can acquire, after one recollision, a kinetic energy which, when averaged over one laser cycle reads

$$\langle E_{kin}\rangle=\frac{1}{2}\left[\frac{F_0}{\omega}[2\cos(\omega t_1)-\cos(\omega t_0)]\mp\sqrt{2E_{kin}(t_0)}\right]^2. \tag{18}$$

Numerically, one finds that the maximum energy is reached by electrons ejected at $\omega t_0=155.2°$. One has $E_{kin,max}\approx9.2U_p$, a value that coincides almost exactly with the end of the structure in the ATI spectrum at this intensity, see Fig. 1.

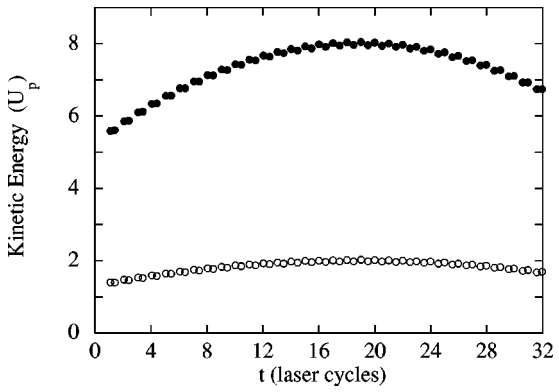

FIG. 7. Kinetic energies as a function of return times t_1 of an electron following the trajectory labeled *A* in Fig. 6(b). Open circles, return kinetic energy at $x=0$, see Eq. (17); filled circles, final kinetic energy after recollision, see Eq. (18).

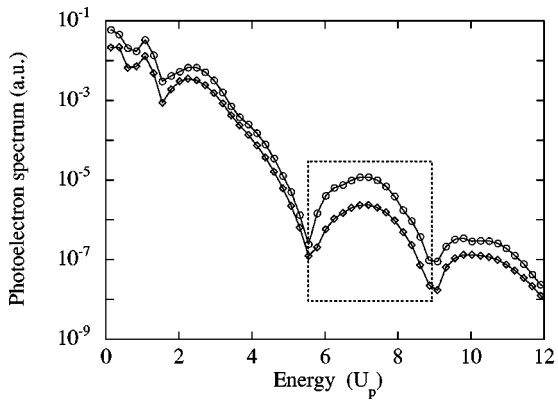

FIG. 8. Photoelectron spectra for the long-range potential Eq. (1), for $I=1.145\times10^{14}$ W cm^{-2} and for two different pulse durations. Open circles, 32 cycles; diamonds, 16 cycles.

To illustrate the case of an (almost) periodic trajectory, we have followed in time the history of the electrons released at $\omega t_0 \approx 145°$ [trajectory A in Fig. 6(b)]. They can acquire an instantaneous kinetic energy $1.4U_p \leqslant E_{kin}(t_1)|_{x=0} \leqslant 2U_p$, when they revisit the origin, twice per cycle, see Fig. 7. In the course of a given recollision, depending on the phase of the laser, they can undergo either an elastic collision, with no change of energy, or an inelastic collision, in the course of which they can gain further energy. A third possibility is that it recombines in the potential well, a process which replenishes the ground-state population and leads to harmonic emission [16]. Regarding ionization, the most interesting point is that, after an inelastic, energy-gaining recollision, the electrons following these trajectories can acquire final energies comprised between $5.5U_p \leqslant E_{kin} \leqslant 8U_p$, i.e., within the energy range where the high-energy structures are observed. Other trajectories can reencounter the origin a large number of times. Our simulations indicate that they end with energies comprised between $5.5U_p \leqslant E_{kin} \leqslant 9.2U_p$.

A direct consequence of the existence of this class of rescattering events is the probability that the electron experiences an energy-gaining recollision grows with the number of returns to the origin and, consequently, with the duration of the laser pulse. This scenario is much different from the case where only one or a few recollisions can take place, early during the pulse. This remark leads to the prediction that the magnitudes of the high-energy structures could grow nonlinearly with the pulse duration. This interesting property is confirmed by quantal simulations based on the resolution of the TDSE. In Fig. 8 are shown two ATI spectra, computed for two pulse durations, at an intensity $I=1.145\times10^{14}$ W cm^{-2}, i.e., where a resonance with the state $n=6$ has been identified. The spectrum labeled (a) is the one obtained for a trapezoidal pulse with a 16-cycle flat-top, while the one labeled (b) is obtained for a 32-cycle flat-top. As expected, the spectrum (b) is located above (a) and, the total ionization probability growing approximately linearly in time so long as one can neglect the depletion of the ground state, the area comprised under (b) should be close to twice as large as that under (a). However, this general rule applies only for the electrons ejected either directly or after a few returns to the origin and it should not hold if the electrons can revisit the origin a large number of times. This is precisely what has happened for those that have been emitted with energies comprised between $5.5U_p \leqslant E_{kin} \leqslant 9.2U_p$. This remarkable feature is verified by computing the areas comprised under different parts of the spectra.

Let $P_N(E_{kin})$ be the envelope function of the ATI spectrum as a function of E_{kin}, for a pulse with *N*-cycle duration and let define the integrals as

$$J_N = \int_0^{12U_p} dE_{kin} P_N(E_{kin}),$$

$$K_N = \int_0^{5.5U_p} dE_{kin} P_N(E_{kin}),$$

$$L_N = \int_{5.5U_p}^{9.2U_p} dE_{kin} P_N(E_{kin}), \tag{19}$$

where the integration range in the latter spans the region where the high-energy structure is found. The corresponding ratios for the pulse durations considered turn to be

$$R_J = \frac{J_{32}}{J_{16}} \approx 1.95,$$

$$R_K = \frac{K_{32}}{K_{16}} \approx 1.84,$$

$$R_L = \frac{L_{32}}{L_{16}} \approx 3.26. \tag{20}$$

This shows that for the whole spectrum, that is dominated by the contributions of the slow electrons, and for the energy range not including the high-energy structure, one finds a value only slightly smaller than 2. The difference can be ascribed to the depletion of the ground state which becomes significant at longer times. In contrast, the ratio is significantly larger than 2 in the energy range spanning the region where the enhancement is observed. The nonlinear dependence on time of the magnitude of the latter is clearly dem-

onstrated, a result that confirms the essential role of the orbits in which the electrons can revisit the origin a large number of times. We note that the importance of the role of these periodic (or quasiperiodic) orbits has been stressed, not only in the ATI spectra but, also, in other laser-induced processes, such as nonsequential double ionization in multielectron atoms, see Ref. [14], and harmonic generation [15,16].

To summarize the results obtained in this section, we have shown that in a long-range potential supporting a large number (in principle infinite) of excited states, multiphoton resonances on some of these states are responsible for the enhancements observed in the ATI spectra. It remains to explain why several sets of numerical and analytical simulations, based on the use of a zero range (δ-function) potential, supporting only one bound state, can also reproduce a similar behavior [10,11,13,14]. We shall address this question in the following section.

III. SHORT-RANGE POTENTIALS: PHOTOIONIZATION DYNAMICS IN THE ABSENCE OF RYDBERG STATES

A. Time-dependent Schrödinger equation (TDSE) treatment

Short-range potentials, with an exponentially decreasing tail, support only finite numbers of states. They can mimic the behavior of negative-ion species. In order to investigate the dynamics of strong-field photoionization in such systems, we have chosen two different short-range potentials, namely, a $1D$ ''soft-Yukawa'' potential, that has a Yukawa-like asympotic behavior and is smoothed at the origin and a Pöschl-Teller potential, see for instance, Ref. [36]. We mention that it is for practical reasons, related to the numerical stability of the grid computations, that we have not discussed the idealized case of a one-dimensional δ-function potential.

1. Soft-Yukawa potential

We have first considered the case of a soft-Yukawa potential, of the general form:

$$V_Y(x) = -a\frac{e^{-\alpha\sqrt{b+x^2}}}{\sqrt{c+x^2}}, \tag{21}$$

where the choice of a set of parameters a,b,c, and α determines the depth (a), the smoothness at the origin (b and c), and the range (α) of the potential. One can then select the number and energies of the bound states supported by this potential. For instance, with $a=1.065$, $b=0.1$, $c=1.41$, and $\alpha=0.5$, the system possesses two bound states with energies $\epsilon_0=-0.3938$ a.u. and $E_1=-0.0283$ a.u., and opposite parities. With the same laser parameters as above, the phenomenon of channel-closing for 10, 11, and 12 photons occurs at intensities $I_{10}\approx 8.42\times 10^{13}$ W cm^{-2}, $I_{11}\approx 1.10\times 10^{14}$ W cm^{-2}, and $I_{12}\approx 1.36\times 10^{14}$ W cm^{-2}, respectively. We mention that these intensities do not coincide with the values given by the approximate relation Eq. (4), as they are computed from a Floquet treatment which provides the exact dressed ground-state energy, i.e., including the ac-Stark shift, see below.

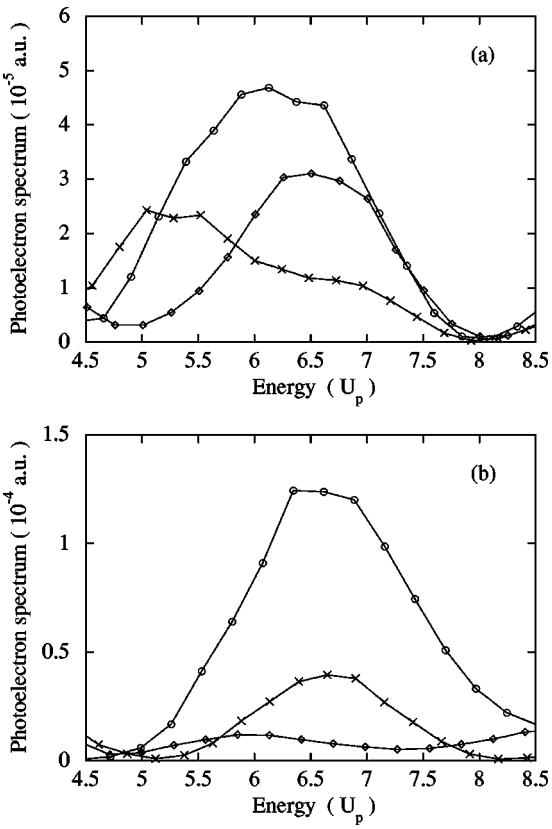

FIG. 9. Envelopes of the high-energy part of the photoelectron spectra for the soft-Yukawa potential Eq. (21) and for $\omega=0.0577$ a.u. (a) Diamonds, open circles, and crosses correspond to intensities of 1.08×10^{14} W cm^{-2}, 1.10×10^{14} W cm^{-2}, and 1.12×10^{14} W cm^{-2}, respectively. (b) Diamonds, open circles, and crosses correspond to intensities of 9.50×10^{14} W cm^{-2}, 9.95×10^{14} W cm^{-2}, and 1.06×10^{14} W cm^{-2}, respectively.

As shown in Fig. 9(a), a high-energy enhancement, equivalent to those observed in the preceding section, is found. This enhancement reaches its maximum at an intensity slightly lower than I_{11}, i.e., just before the 11-photon channel-closing. This is very similar to what is found in calculations made for a (three-dimensional) δ-function potential, Refs. [10,11,13]. However, we do not find any structure in the intensity ranges around the 10- and 12-photon channel closings. The fact that the parity of the number N of photons involved plays an essential role agrees with the results of the mentioned references. There is, however, an important difference regarding the parity of N: In our $1D$ simulations for this potential, it is odd, while for the $3D$, δ potential, it is even. It is likely that the origin of this difference lies in the fact that the number of bound states, with alternating parities, supported by our potential, plays a determining role. We shall come back to this point later.

More interestingly, when exploring a wider intensity range, it turns out that another high-energy enhancement shows up at $I\approx 9.95\times 10^{13}$ W cm^{-2}, i.e., far from any channel closing, see Fig. 9(b). This is in marked contrast with the case of the δ-function potential, where no enhancements at intensities other than those associated to channel closings have been reported yet.

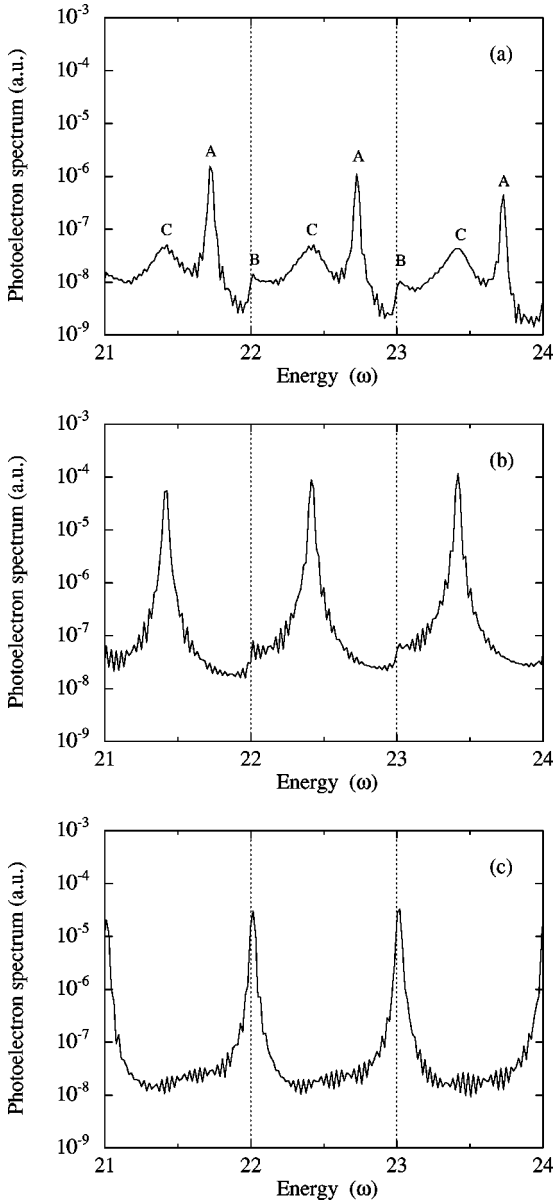

FIG. 10. Structure of a set of ATI peaks for the soft-Yukawa potential Eq. (21) and for $\omega=0.0577$ a.u. (a), (b), and (c) correspond to intensities of 9.13×10^{13} W cm^{-2}, 9.95×10^{13} W cm^{-2} [when the enhancement is observed in Fig. 9(b)], and 1.10×10^{14} W cm^{-2} [when the enhancement is observed in Fig. 9(a)], respectively.

To uncover the origin of these enhancements, it is helpful to look at the details of the ATI spectra in the energy range of interest. A selected set of these spectra are shown in Fig. 10. Figure 10(a) is for an intensity not too close from resonance, in order not to blurr the substructure of the peaks. Here one can check that each ATI peak is made of three subcomponents. This is quite surprising at first, in view of the fact that the potential supports only one excited state. Indeed, in addition to that (labeled A) associated to the nonresonant transition one observes two other subpeaks. One of them (labeled B) is located *almost* exactly at threshold energies $E_{kin,N+S}=S\omega$, where N is the exact number of photons needed to ionize the ground state and S is the number of photons absorbed in excess. Regarding the third one (labeled C) it could be associated to a resonance on the excited state, similar to those observed above. Increasing the intensity, one observes that the peak (A) moves towards lower kinetic energies, as expected, while the other ones do not move appreciably. And again, much similarly to what was found in the preceding section, the magnitude of a given peak is significantly enhanced at intensities where (A) merges with either (C) or (B). This takes place at $I\approx9.95\times10^{13}$ W cm^{-2}, see Fig. 10(b), for peak (C) and at $I\approx1.10\times10^{14}$ W cm^{-2}, see Fig. 10(c), for peak (B). These intensities coincide with those at which enhancements were found, in agreement with the results shown in Fig. 10.

Clearly, it is *a priori* tempting to ascribe peaks (B) to a channel-closing phenomenon and peaks (C) to a resonance on the excited state. In order to discuss these possibilities, we have performed a Floquet analysis designed to search for the states that could be involved in these processes. However, before doing, we present the results obtained for another potential well, supporting only one bound state.

2. Pöschl-Teller potential

The short-range Pöschl-Teller potential is of the general form [36]:

$$V_{P-T}(x)=-\frac{a}{ch^2(\alpha x)}, \tag{22}$$

where the choice of parameters a and α determines the ground-state energy and the number of bound states. Here, for $a=0.828$ and $\alpha=0.978$, there is only one bound state with energy $\epsilon_0=-0.3938$ a.u., i.e., the same as for the soft-Yukawa potential discussed previously. For field parameters as before, the intensities corresponding to channel closings involving 10, 11, and 12 photons should occur at $I_{10}\approx8.37\times10^{13}$ W cm^{-2}, $I_{11}\approx1.105\times10^{14}$ W cm^{-2}, and $I_{12}\approx1.36\times10^{14}$ W cm^{-2}, respectively. Again, these intensities were derived from a Floquet analysis and they differ slightly from the values given by Eq. (4).

For this potential, one observes the presence of enhancements in the high-energy part of the ATI spectra, at intensities close to (in fact, just below) I_{10} and I_{12}. This is similar to the result found with the soft-Yukawa potential and also to the findings reported in Refs. [10–14]. No similar effect is observed at intensities close to I_{11}, also in agreement with these references. However, most interestingly, we have also found a very significant enhancement, see Fig. 11, at $I_{crit}\approx9.46\times10^{13}$ W cm^{-2}, i.e., located far from any channel-closing intensity. Since the considered model potential does not support any excited state, it is not easy to account for the presence of this enhancement from the present TDSE treatment. Again, in order to uncover the origin of the phenomenon, we have performed a Floquet analysis of the dressed spectrum of the system.

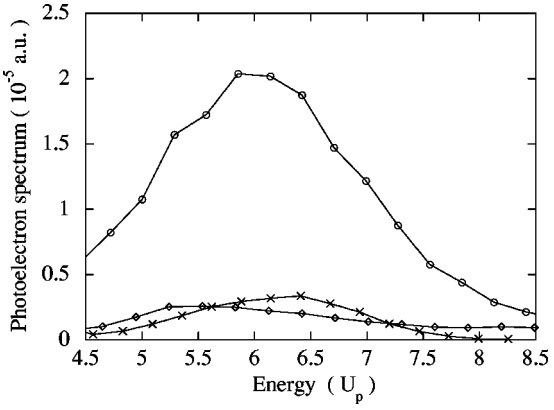

FIG. 11. Envelopes of the high-energy part of the photoelectron spectra for the Pöschl-Teller potential, Eq. (22). Diamonds, open circles and crosses correspond to intensities of 9.10×10^{13} W cm^{-2}, 9.46×10^{13} W cm^{-2}, and 1.02×10^{14} W cm^{-2}, respectively.

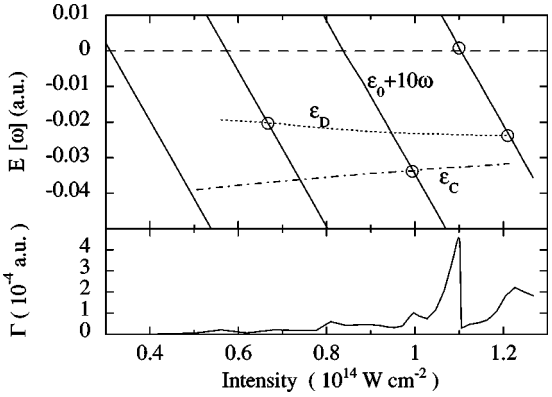

FIG. 12. Excerpt of the Floquet spectrum for the soft-Yukawa potential, Eq. (21). Upper panel, real part, modulo ω, of the quasienergies. LIS are labeled *C* (see Fig. 10) and *D*. We have indicated the crossings with the ground state giving rise to a resonance. Lower panel, width of the ground state, see Eq. (23).

B. Floquet quasienergies treatment: Role of laser-induced states

The sturmian basis introduced above to solve the system of equations (7), verified by the Fourier-Floquet components of the wave function, has revealed itself to be inadequate in the case of the short-range potentials considered in this section. We have used instead a technique proposed by Bardsley *et al.* [37]. In short, it consists in propagating in time, over one laser period, the matrix $U(t)$ representing the propagator which obeys the operator equation:

$$U(t+T)=\exp\left[-i\left(E-i\frac{\Gamma}{2}\right)T\right]U(t), \tag{23}$$

where Γ stands for the width of a state with quasienergy E. Using a basis of particle-in-a-box wave functions, together with the complex scaling and a standard split-operator propagation technique, one can recover the Floquet quasienergies from the diagonalization of the matrix $U(T_L)$, where T_L is the cycle duration. We turn now to the presentation of the Floquet spectra for the two short-range potentials we have considered.

1. Floquet quasienergies for the soft-Yukawa potential

In Fig. 12, we present an excerpt of the Floquet spectrum computed for the same frequency and intensities as discussed above for the the ''soft-Yukawa'' potential. We have represented the quasienergies with real parts located below (and close to) the ionization threshold. Note that we have only shown the states with widths $\Gamma\leqslant2.5\times10^{-2}$ a.u., i.e., with lifetimes larger than $\tau\approx T_L$. Note that the only excited state disappears, drowned into the continuum at $I\approx3\times10^{13}$ W cm^{-2}. Beyond this intensity, we have not been able to follow its trajectory in the complex plane with our numerical calculations. We note that a similar behavior has also been found in other simulations [37]. More interestingly, beyond $I\approx5\times10^{13}$ W cm^{-2}, two new states labeled (*C*) and (*D*) show up. They can be identified as laser-induced states (LIS) that have been documented in the literature [18,19]. Their complex energies depend on the intensity and it turns out that those with long enough lifetimes can play a determining role in the ionization dynamics.

In fact, they can give rise to resonances, much like the Rydberg states, considered in the preceding section. As shown in Fig. 12 (upper pannel), a crossing, associated with a 10-photon resonance between the ground state and state (C), takes place at $I\approx9.95\times10^{13}$ W cm^{-2}, which coincides with the intensity at which an enhancement is observed in the ATI spectrum, as explained above in Sec. III A 2. However, as previously discussed, there is also an enhancement at $I\approx1.10\times10^{14}$ W cm^{-2}, i.e., just before the channel-closing intensity I_{11} that is indicated on the figure. The occurrence of an resonant transition is confirmed by following the intensity dependence of the width of the ground state that is reported in the Fig. 12 (lower pannel). There, one observes that the width exhibits a sharp maximum slightly before I_{11}. In fact, our simulations point to the presence of an LIS that would be located just above the threshold limit, with a real part $\mathrm{Re}(E)\approx6.7\times10^{-4}$ a.u. We must mention, however, that for those states located so close to the singularity associated to the threshold, it is very difficult to determine a reliable estimate for their imaginary part. This is because a precise determination would require the use of huge integration boxes. As we shall show next, this behavior is also observed in the case of a narrow potential well that does not support any excited state.

2. Floquet quasienergies for the Pöschl-Teller potential

An excerpt of the relevant Floquet spectrum for the Pöschl-Teller potential in Eq. (22), and the same set of parameters as in Sec. III A 2, is shown in Fig. 13. The potential supports only one bound state. Here, two LIS, labeled (A) and (B), do cross with the shifted ground state at intensities in the range considered above, beyond $I\approx3\times10^{13}$ W cm^{-2}. For instance, there is a crossing with the LIS labeled (A), at $I_{crit}\approx9.46\times10^{13}$ W cm^{-2}, corresponding exactly with the enhancement shown in Fig. 11. This indicates that this enhancement can be ascribed to the same multiphoton resonant mechanism that has been identified for

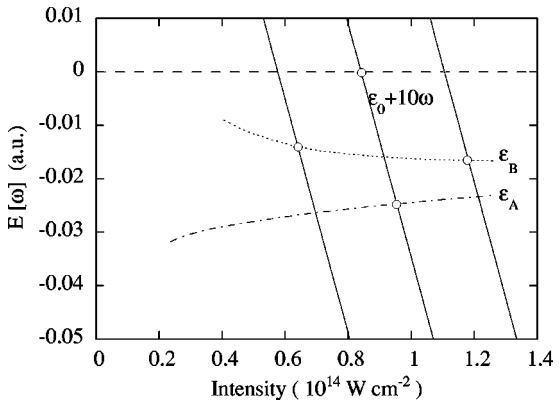

FIG. 13. Excerpt of the Floquet spectrum for the Pösch-Teller potential, Eq. (22). Real part, modulo ω, of the quasienergies. LIS are labeled *A* and *B*. We have indicated the crossings with the ground state giving rise to a resonance.

the long-range and soft-Yukawa potentials. Here, the difference is that there is no possible ambiguity regarding the role of the LIS. We mention that the other crossings give also rise to enhancements, though less marked than this one.

Interestingly, there is also an enhancement at an intensity $I_{crit} \approx 8.37 \times 10^{13}$ W cm^{-2}, corresponding to the 10-photon channel closing. Much similarly to what was observed for the soft-Yukawa potential, our simulations point to the presence of a zero-energy LIS that is located just above the ionization threshold. However, for the same reasons as explained in the case of the soft-Yukawa potential, we have been unable to locate accurately this state with a real part of the energy of the order of 10^{-4} a.u. We note that, here, this zero-energy LIS is of even parity, as indicated by the 10-photon crossing with the ground state. The fact that no similar resonances are observed at the 9th and 11th channel closings is likely to be related to the parity of the states considered.

These results might explain why other simulations, performed for a zero-range δ-function potential, via an *S*-matrix formalism, exhibit enhancements at intensities close to those corresponding to channel closings [10–14]. We note that the model δ-function potential used in these simulations is three dimensional, while our calculations have been performed for $1D$ model potentials. The fact that parity matters is a signature of the multiphoton nature of the process responsible for the enhancements. As we shall show in a forthcoming paper, it turns out that similar features are also found when simulating high-order harmonic spectra from this class of potentials [16].

IV. DISCUSSION AND CONCLUSIONS

In this paper, we have addressed the question of the physical origin of remarkable enhancements observed in the high-energy part of the ATI spectra. The main question at hand was to explain why two *a priori* distinct classes of physical mechanisms could be invoked to account successfully for the presence of these enhancements in the spectra. One class of simulations links them to the occurrence of multiphoton resonances involving the Rydberg states in model atomic potentials. Meanwhile, another set of simulations ascribes them to channel closings, in zero-range model potentials, with no excited state. The objective of the present paper was to understand why these two sets of simulations could reproduce such a conspicuous behavior in the high-energy part of the ATI spectra.

Our own investigations have been based on the resolution of the TDSE for one-dimensional model potentials, either long-range (soft-Coulomb) or short-range (soft-Yukawa and Pöschl-Teller). The numerical results for the ATI spectra, as deduced from a TDSE treatment, have been interpreted with the help of a Floquet and of a classical trajectory analysis. The explanation suggested by these analyses points to the essential role of multiphoton resonances involving excited states. This agrees with the observation made previously by Muller *et al.* [7–9]. The electrons involved in the enhancements are those which, being ejected from these states, recollide with the ionic core. As we have shown, the highly nonlinear dependence of the enhancements on the laser intensity is linked to the existence of oscillating electron trajectories that revisit the origin twice per laser cycle. As they start with a nonzero initial kinetic energy, they still have nonzero instantaneous kinetic energies when they come back to the origin. Then, if they do not recombine while being scattered by the potential, they can either gain further energy, thus contributing to the high-energy part of the ATI spectrum, or be elastically scattered and recollide again. In the latter case, the same scenario is repeated, a situation which implies that the probability for an electron to reach the plateau region grows with the number of allowed recollisions. This leads to the prediction that the magnitudes of the enhancements should grow nonlinearly with the duration of the laser pulse, see Eqs. (18). We believe that this prediction should be amenable to experimental verifications.

Regarding the case of short-range potentials, adapted to the description of negative ions, our analysis shows that laser-induced states (LIS) can play the same role as excited states in atoms. Accordingly, strong enhancements are found in the simulations of the ATI spectra, whenever there is a multiphoton resonance between the ground state and one of these LIS. On the other hand, we have also found a similar behavior at intensities close to associated to channel closings. This is in global agreement with previous findings, in calculations performed with the help of a (three-dimensional) δ-function potential [10–14]. Moreover, our numerical simulations seem to indicate the existence of LIS located just above the ionization threshold. However, because of numerical uncertainties, we cannot ascertain with accuracy the location of the quasienergy of these dressed states in the complex plane.

In conclusion, our results confirm unambiguously the essential role of multiphoton resonances being at the origin of the enhancements found in the ATI at intensities around $\approx 10^{14}$ W cm^{-2} for a Ti:sapphire laser, i.e., at the border between the multiphoton and the tunneling regime. However, we have found that the mechanism at work is quite different from that accounting for the structures of the ATI peaks in the low-energy part of the spectra (the so-called Freeman

resonances). Here, another essential ingredient is the existence of electron trajectories which can experience multiple recollisions with the origin. In our opinion, put together, the resonance and the multiple-recollision mechanisms account for the essential features of the phenomenon, as it has been observed in atoms. On the other hand, for short-range model potentials, we have confirmed the existence of a channel-closing-like mechanism. In addition, we have also found that, in some cases, LIS could play the role of excited states in atoms. We believe that this set of results should motivate further investigations in both theory and experiments Note that a companion paper is devoted to the application of the above presented analysis to the process of harmonic generation that takes place in the same intensity regime [16].

ACKNOWLEDGMENTS

The Laboratoire de Chimie Physique-Matière et Rayonnement is a Unité Mixte de Recherche, Associée au CNRS, UMR 7614, and is Laboratoire de Recherche Correspondant du CEA, LRC Grant No. DSM-98-16. Parts of the computations have been performed at the Centre de Calcul pour la Recherche (CCR, Jussieu, Paris) and at the Institut du Développement et des Ressources en Informatique Scientifique (IDRIS).

[1] G.G. Paulus, W. Nicklich, H. Xu, P. Lambropoulos, and H. Walther, Phys. Rev. Lett. **72**, 2851 (1994).
[2] M.P. Hertlein, P.H. Bucksbaum, and H.G. Muller, J. Phys. B **30**, L197 (1997).
[3] P. Hansch, M.A. Walker, and L.D. van Woerkom, Phys. Rev. A **55**, R2535 (1997).
[4] The ponderomotive energy $U_p = q^2 F_0^2/(4m\omega^2)$, is the averaged kinetic energy of an electron set in forced motion by a field with amplitude F_0 and frequency ω. It is proportional to the laser intensity $I_L = \frac{1}{2}\sqrt{\epsilon_0/\mu_0}|F_0|^2$.
[5] E. Cormier, D. Garzella, P. Breger, P. Agostini, G. Chériaux, and C. Leblanc, J. Phys. B **34**, L9 (2001).
[6] G.G. Paulus, W. Becker, W. Nicklich, and H. Walther, J. Phys. B **27**, L703 (1994).
[7] M.J. Nandor, M.A. Walker, L.D. van Woerkom, and H.G. Muller, Phys. Rev. A **60**, R1771 (1999).
[8] H.G. Muller and F.C. Kooiman, Phys. Rev. Lett. **81**, 1207 (1998).
[9] H.G. Muller, Phys. Rev. A **60**, 1341 (1999); Phys. Rev. Lett. **83**, 3158 (1999); Opt. Eng. (Bellingham) **8**, 44 (2001).
[10] G.G. Paulus, F. Grasbon, H. Walther, R. Kopold, and W. Becker, Phys. Rev. A **64**, 021401(R) (2001).
[11] R. Kopold, W. Becker, M. Kleber, and G.G. Paulus, J. Phys. B **35**, 217 (2002).
[12] A. Lohr, M. Kleber, R. Kopold, and W. Becker, Phys. Rev. A **55**, R4003 (1997); D.B. Milošević and F. Ehlotzky, *ibid.* **58**, 3124 (1998); S.P. Goreslavskiĭ and S.V. Popruzhenko, JETP **90**, 778 (2000).
[13] B. Borca, M.V. Frolov, N.L. Manakov, and A. F Starace, Phys. Rev. Lett. **88**, 193001 (2002).
[14] S.V. Popruzhenko, P.A. Korneev, S.P. Goreslavski, and W. Becker, Phys. Rev. Lett. **89**, 023001 (2002).
[15] C. Figueira de Morisson Faria, R. Kopold, W. Becker, and J.M. Rost, Phys. Rev. A **65**, 023404 (2002).
[16] R. Taïeb, V. Véniard, J. Wassaf, and A. Maquet (unpublished).
[17] J. Wassaf, V. Véniard, R. Taïeb, and A. Maquet, Phys. Rev. Lett. **90**, 013003 (2003).
[18] R. Bhatt, B. Piraux, and K. Burnett, Phys. Rev. A **37**, 98 (1988).
[19] J.C. Wells, I. Simbotin, and M. Gavrila, Phys. Rev. Lett. **80**, 3479 (1998); see also the discussion: P. Schlagheck, K. Hornberger, and A. Buchleitner, *ibid.* **82**, 664 (1999); J.C. Wells, I. Simbotin, and M. Gavrila, *ibid.* **82**, 665 (1999).
[20] Q. Su and J.H. Eberly, Phys. Rev. A **44**, 5997 (1991).
[21] K.J. Schafer and K.C. Kulander, Phys. Rev. A **42**, 5794 (1990).
[22] W.G. Greenwood and J.H. Eberly, Phys. Rev. A **43**, 525 (1991).
[23] J. Wassaf, thesis Université Pierre et Marie Curie, Paris, 2002 (unpublished).
[24] The variation of $E_{kin,N}$ as $-U_p$ is only approximate. In fact, the difference between the ac-Stark shifted ground-state energy and the ionization limit varies as $-1.03\times U_p$. This more precise dependence is derived from the Floquet analysis presented below.
[25] R. Freeman, P.H. Bucksbaum, H. Milchberg, S. Darack, D. Schumacher, and M.E. Geusic, Phys. Rev. Lett. **59**, 1092 (1987).
[26] One reports usually the populations computed at times when the field is zero during the cycle.
[27] J.H. Shirley, Phys. Rev. **59**, B979 (1965).
[28] A. Maquet, S. Chu, and W.P. Reinhardt, Phys. Rev. A **27**, 2946 (1983).
[29] T. Millack, V. Véniard, and J. Henkel, Phys. Lett. A **176**, 433 (1993).
[30] M. Dörr, R.M. Potvliege, and R. Shakeshaft, Phys. Rev. A **41**, 558 (1990).
[31] M. Rotenberg, Adv. At. Mol. Phys. **6**, 233 (1970).
[32] A. Maquet, Phys. Rev. A **15**, 1088 (1977).
[33] R.M. Potvliege, Comput. Phys. Commun. **114**, 42 (1998).
[34] W.C. Liu and C. W Clark, J. Phys. B **25**, L517 (1992); C.W. Clark, *ibid.* **30**, 2517 (1997).
[35] G.G. Paulus, W. Becker, and H. Walther, Phys. Rev. A **52**, 4043 (2001).
[36] S. Flügge, *Practical Quantum Mechanics* (Springer, Berlin, 1971).
[37] J.N. Bardsley, A. Szöke, and M.J. Comella, J. Phys. B **21**, 3899 (1988).